

Impurity-induced bound states as a signature of pairing symmetry in multiband superconducting CeCu_2Si_2

Dong-Dong Wang¹, Bin Liu^{1,†}, Min Liu², Yi-Feng Yang^{2,3,4,‡}, Shi-Ping Feng⁵

¹Department of Physics, Beijing Jiaotong University, Beijing 100044, China

²Beijing National Laboratory for Condensed Matter Physics and Institute of Physics, Chinese Academy of Sciences, Beijing 100190, China

³University of Chinese Academy of Sciences, Beijing 100049, China

⁴Collaborative Innovation Center of Quantum Matter, Beijing 100190, China

⁵Department of Physics, Beijing Normal University, Beijing 100875, China

Corresponding authors. E-mail: [†]liubin@bjtu.edu.cn, [‡]yifeng@iphy.ac.cn

Received July 25, 2018; accepted July 31, 2018

The notion of multiband superconductivity with dominant two-gap features has been recently applied to the unconventional superconductor CeCu_2Si_2 for challenging the previously accepted concept of nodal d -wave pairing. In the proposed study, the realistic multiband Fermi surface topology of CeCu_2Si_2 was obtained through first-principles calculations, and analysis was conducted with an effective two-band hybridization model including detailed band structure. Within the T -matrix approximation, the obtained calculation results show that different pairing candidates, including fully gapped s -wave, loop-nodal s -wave, and d -wave pairings, could yield qualitatively distinct features characterized by impurity-induced bound states. These features can be verified through high-resolution scanning tunneling microscopy or spectroscopy and provide corroborative justification that would be beneficial for the ongoing research regarding the superconducting gap symmetry of CeCu_2Si_2 at ambient pressure.

Keywords heavy-fermion superconductivity, pairing symmetry, impurity effect, local density of states

1 Introduction

Recently, superconducting (SC) gap symmetry of the heavy-fermion superconductor CeCu_2Si_2 has attracted considerable attentions. As the first unconventional superconductor discovered in 1979 [1], CeCu_2Si_2 has long been thought to be a single-band nodal d -wave superconductor at ambient pressure, which has been naturally associated with an antiferromagnetic quantum critical point beneath the SC dome and thereby provides a model phase diagram for unconventional superconductivity [2, 3]. The d -wave pairing has also been indirectly evidenced by the subsequent specific heat measurement [4, 5], the nuclear magnetic/quadrupole resonance (NMR/NQR) [6–8] and the neutron scattering experimental detections [9]. The only remaining discrepancy seems to be the exact d -wave gap structure, either $d_{x^2-y^2}$ or d_{xy} [10, 11]. However, this view is recently challenged by some latest measurements. In contrast to the nodal d -wave pairing, recent specific heat measurement down to very low temperature on CeCu_2Si_2 at ambient pressure provides clear evidence of multiband superconductivity with a two-gap structure [12, 13], which has been further convinced by subsequent scanning tunneling microscopy (STM/STS) [14] and London penetra-

tion depth measurements [15, 16]. Theoretical calculations using a multiband model afterwards suggest that the superconductivity might be either nodeless s^\pm -wave [17], or loop-nodal s -wave [18], in contrast to the previous conclusion of d -wave based on single band calculations.

Despite that tremendous efforts have been made in the past decades, direct experimental detections of the pairing symmetry are still lacking. While the well-known angle-resolved photoemission spectroscopy (ARPES) could provide an exact mapping of the band structures, it is, however, limited by the energy resolution [19]. This makes it difficult to apply for the heavy fermion superconductor, which typically has a SC transition temperature of a few Kelvin and is indiscernible in current ARPES measurement [20–22]. The exact form of gap symmetry in CeCu_2Si_2 remains to date elusive. Because of the particular Fermi surface topology of CeCu_2Si_2 , conventional phase-sensitive measurements cannot be readily applied to detect the pairing symmetry and differentiate the various proposals.

Fortunately, new spectroscopic technique has recently been developed based on high-resolution STM [23], where heavy-fermion quasiparticle interference (QPI) could be used to determine the quasiparticle band dispersions at much lower temperature, and measure within μeV en-

ergy scale the detailed \mathbf{k} -space gap functions. As a result, both QPI and local pair-breaking experiments have been successfully applied to the heavy-fermion superconductor CeCoIn₅ to identify its $d_{x^2-y^2}$ pairing symmetry [24–27]. In this paper, we theoretically extend such idea to CeCu₂Si₂ as an alternative way to distinguish its SC gap structure. Considering the possibly multiband nature of superconductivity in CeCu₂Si₂, we study the problem within an effective model with two hybridization bands obtained from density function calculations with local density approximation taking into account the Coulomb interaction of the Ce f -electrons and the spin-orbit coupling (LDA+ U). Our results based on T -matrix approximation show that both the loop-nodal s -wave and d -wave pairing can give rise to impurity-induced intra-gap bound states. While the intra-gap states for loop-nodal s -wave pairing have energies far away from the Fermi energy irrespective of the impurity scattering strength. This is markedly different from the features shown in the d -wave one, where a nearly zero-energy impurity-induced bound state appears for weak impurity scattering. We also reveal that in the case of fully gapped nodeless s -wave, NO intra-gap impurity states can be induced by a nonmagnetic impurity when only considering the intra-band impurity scattering, while impurity-induced bound state via the inclusion of the inter-band impurity scattering could identify the sign changing or not for the nodeless s^{++} - and s^{\pm} -wave pairings. These qualitatively distinct features can be captured in STM and therefore provide a useful guide for unambiguous experimental justification of these different scenarios to solve this highly debated issue of pairing symmetry in heavy-fermion superconductor CeCu₂Si₂.

2 Local density approximation and T -matrix approach

Since the realistic Fermi surface (FS) topology is crucial for understanding the unconventional superconductivity, we firstly perform band structure calculations for CeCu₂Si₂ based on LDA+ U . The resulting three-dimensional (3D) FSs for the effective Coulomb interaction $U_{eff} = 5$ eV as shown in Fig. 1(a) includes a corrugated-cylindrical heavy electron sheet around X point, and complex inner hole sheets, in reasonable agreement with previous calculations [18, 28]. The typical 2D FSs of our hybridization band model for $k_z = 1.8\pi/c$ is depicted in Fig. 1(b), where the hybridization heavy electron FS around (π, π) is denoted as β -band and the light hole FSs around $(0, 0)$ denoted as α -band. Fig. 1(c) plots the corresponding band structure, where two heavy-fermion bands clearly appear due to the hybridization from the spin screening of the Kondo lattice at low temperatures as indicated by the cycles, and the extreme flatness of the heavy β -band near the chemical potential represents typical f -characters. As a consequence, the two peaks

in the density of state (DOS) indicated by the arrows in Fig. 1(d) stem from above hybridization between the heavy and light bands. We also note that the heavy β -band in Fig. 1(d) has a much larger density of state near the Fermi energy, and maybe dominate the low energy properties, which is why most earlier work were based only on the single-band scenario for studying the unconventional superconductivity in CeCu₂Si₂.

We now start with the two hybridization-band model, and introduce a four-component Nambu spinor operator to formulate the bare Green's function in the SC state as

$$\hat{G}_0^{-1}(\mathbf{k}; i\omega_n) = i\omega_n \hat{1} - \begin{pmatrix} E_{\mathbf{k}}^{\alpha} & \Delta_{\mathbf{k}}^{\alpha} & 0 & 0 \\ \Delta_{\mathbf{k}}^{\alpha} & -E_{\mathbf{k}}^{\alpha} & 0 & 0 \\ 0 & 0 & E_{\mathbf{k}}^{\beta} & \Delta_{\mathbf{k}}^{\beta} \\ 0 & 0 & \Delta_{\mathbf{k}}^{\beta} & -E_{\mathbf{k}}^{\beta} \end{pmatrix}, \quad (1)$$

where ω_n is the fermionic Matsubara frequency and $E_{\mathbf{k}}^{\alpha/\beta}$ is the dispersion of the α - and β -bands. Since the two hybridization-bands don't overlap, we in this study only discuss the intraband pairing. The considered pairing symmetry includes nodal $d_{x^2-y^2}$ -wave, loop-nodal s -wave with $\Delta_{\mathbf{k}}^{\alpha/\beta} = \Delta^{\alpha/\beta} \cos k_x \cos k_y$ and nodeless s^{\pm} -wave. Recent specific heat measurement reveals an exponential T -

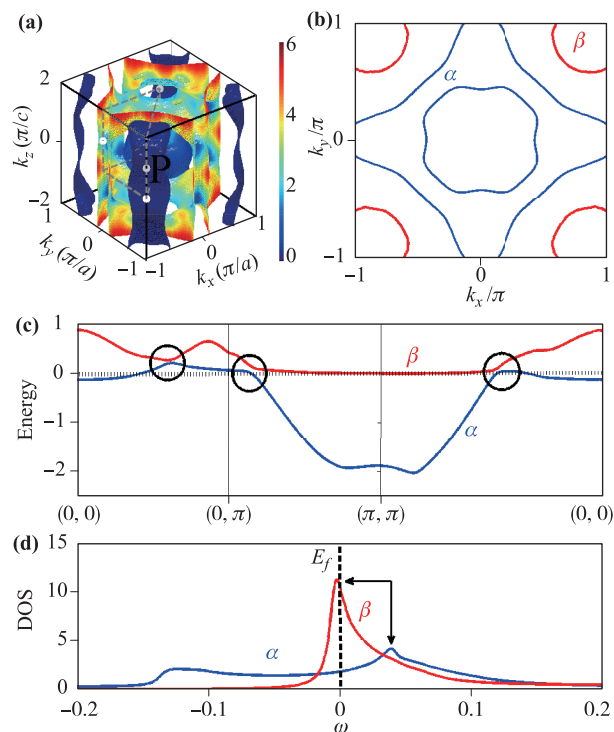


Fig. 1 (a) Calculated 3D Fermi surfaces colored by the Fermi velocity for CeCu₂Si₂ at ambient pressure. (b) The 2D FSs of our hybridization-band model. β and α denote the corrugated-cylindrical heavy electron sheet and complex hole sheets, respectively. (c) Electronic band structures resulted from hybridization as indicated by the cycles. (d) Density of state of the β - and α -bands in the normal state. The two peaks indicated by arrows are direct consequences of the hybridization.

dependence which could be fitted by two gaps with a ratio of about 2.5 [12], and the magnitude of the gap parameters is not clear and need to be determined from further experiments. We thus choose the same gap symmetry for the two bands with $\Delta^\beta/\Delta^\alpha \approx 2$ in following numerical calculations, in that this value cannot qualitatively change our conclusions.

The effect of the impurity scattering can be treated within the T -matrix approach [29]. For simplicity, we consider only a single nonmagnetic impurity and take the potential scattering matrix as the following structure

$$\hat{U} = \begin{pmatrix} U & 0 & V & 0 \\ 0 & -U & 0 & -V \\ V & 0 & U & 0 \\ 0 & -V & 0 & -U \end{pmatrix}, \quad (2)$$

where U and V are the strength for intra-band and inter-band scattering potential, respectively. This yields the full interacting Green's function in real space,

$$\hat{G}(i, j; i\omega_n) = \hat{G}_0(i, j; i\omega_n) + \hat{G}_0(i, 0; i\omega_n)\hat{T}(i\omega_n)\hat{G}_0(0, j; i\omega_n), \quad (3)$$

where $\hat{G}_0(i, j; i\omega_n) = \frac{1}{N} \sum_{\mathbf{k}} e^{i\mathbf{k}\cdot(i-j)} \hat{G}_0(\mathbf{k}; i\omega_n)$ is the real-space bare Green's function and $\hat{T}(i\omega_n) = \hat{U}[\hat{1} - \hat{G}_0(0, 0; i\omega_n)\hat{U}]^{-1}$ is the T -matrix that has incorporated all the scattering processes. The local density of state (LDOS) can then be evaluated as

$$\rho(i, \omega) = -\frac{1}{\pi} \text{Im}[\hat{G}(i, i; i\omega_n)_{11} + \hat{G}(i, i; i\omega_n)_{33} + \hat{G}(i, i; i\omega_n)_{13} + \hat{G}(i, i; i\omega_n)_{31}]_{i\omega_n \rightarrow \omega + i0^+}. \quad (4)$$

This quantity is proportional to the local differential tunneling conductance as measured in STM experiments.

3 Local density of states and impurity-induced bound states

We first discuss the DOS without impurity in the SC state. As shown in Fig. 2, it exhibits two kinds of coherence peaks corresponding to the maximum SC gaps on the two FSs. The coherence peaks near $\pm\Delta_1$ arise from the α -band, while those at higher energies $\pm\Delta_2$ mainly benefit from the β -band. For a nodeless s^\pm -wave, there is no sign change in the SC order parameter within each FS pocket, resulting in the typical U-shape feature in the DOS similar to that in conventional s -wave superconductors [29]. In contrast, the gap structure of the nodal $d_{x^2-y^2}$ -wave has a sign change and its nodal lines cross both FSs enclosed by the α - and β -bands, respectively. As a result, the DOS indicated by the dashed line in Fig. 2 shows a V-shape character, in agreement with recent STM measurement [14]. For the SC gap of loop-nodal s -wave with $\Delta_{\mathbf{k}}^{\alpha/\beta} = \Delta^{\alpha/\beta} \cos k_x \cos k_y$, whose gap structure is given in the inset of Fig. 3(a), the nodal lines as indicated by

the black dashed line only cut the inner α -FS sheet because the radius of the electron β -FS pocket around (π, π) is smaller than $\pi/2$. In this case, the corrugated heavy-electron sheet is fully gapped and only the light-hole sheet has loop nodal points, as proposed in the literature [18]. The resulting DOS is calculated as a dash-dotted line in Fig. 2.

The impurity scattering introduces different local perturbation to the density of states for different SC gap symmetry. Figures 3 and 4 show the LDOS of quasiparticles at the nearest-neighbor (NN) site of the impurity located as the center of the square lattice. To clearly see the intra-gap bound states induced by impurity scattering, we calculate

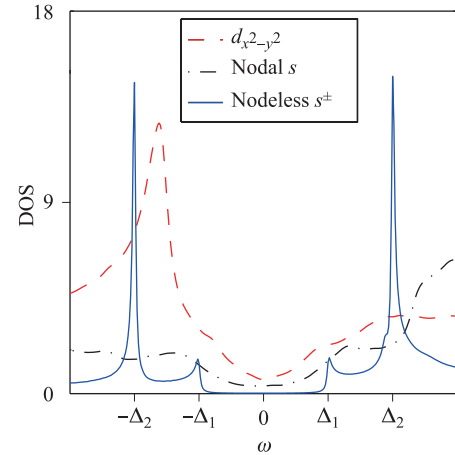


Fig. 2 The density of states in the clean SC state for three gap symmetries, including a nodeless s^\pm -wave (solid line), a nodal $d_{x^2-y^2}$ -wave (dashed line), and a loop-nodal s -wave (dash-dotted line).

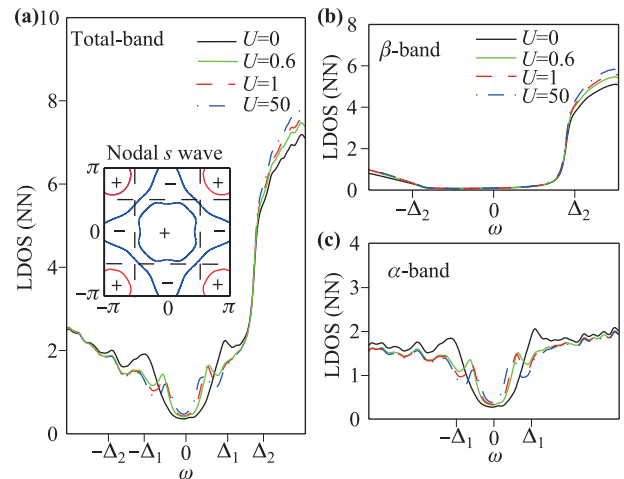


Fig. 3 The LDOS of quasiparticles at the nearest-neighbor (NN) site of the impurity with varying scattering potential for the loop-nodal s -wave with (a) total bands, (b) β -band, and (c) α -band. The inset of (a) is a visualization of the overlap between FSs (solid lines) and the nodal lines (dashed lines) of the gap function; the symbols “+” and “-” denote positive and negative gap values, respectively.

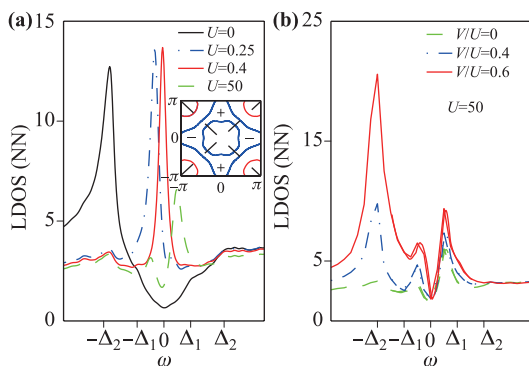


Fig. 4 The LDOS of quasiparticles at NN site for the nodal $d_{x^2-y^2}$ -wave pairing symmetries with only intra-band scattering (a) and with both intra- and inter-band scattering (b). The inset of (a) shows the overlap between the FSs (solid lines) and the nodal lines (dashed lines) of the $d_{x^2-y^2}$ gap function.

the LDOS from the weak (Born approximation) to strong (unitary limit) scattering potential strength. In Fig. 3(a), we plot the LDOS by considering the repulsive impurity scattering for loop-nodal s -wave pairing state. The corresponding gap structure is shown in the inset, where the symbols “+” and “-” describe the positive and negative gap values, respectively. For comparison, the black solid line shows the LDOS in the clean system ($U = 0$). In the presence of a single nonmagnetic impurity, one immediately sees that two intra-gap bound states appear, and nearly do not alter the positions with decreasing scattering strength ($U = 0.6$ with a unit of meV). Here it is surprising to note that the intra-gap bound peaks are far away from the Fermi energy even when the impurity scattering is in the unitary limit ($U = 50$, the dash-dotted line in Fig. 3(a)), in contrast to the situations in high temperature SC cuprates, where the intra-gap bound state is located close to the Fermi energy for strong impurity scattering [29]. Another novel feature is the relatively low spectrum intensities of intra-gap bound states, which can be understood from the nodal gap structure. For loop-nodal s -wave pairing state, the corrugated heavy-electron β -FS is fully gapped. Therefore, no intra-gap bound states can be induced by local nonmagnetic impurity just as plotted in Fig. 3(b) for β -band. The obtained intra-gap bound states are completely generated by the inner light hole α -FS with loop nodal points. As a result, their peak intensities as seen in Fig. 3(c) are very low due to the smaller DOS of the α -band near the Fermi energy as given in Fig. 1(d). Inclusion of the inter-band impurity scattering (not shown here) does not change the above conclusion except that the intensities of intra-gap bound states are enhanced.

Similar calculations have also been performed for the nodal $d_{x^2-y^2}$ -wave and the resulting LDOS for varying repulsive impurity scattering are presented in Fig. 4(a). In comparison with the LDOS of the clean system ($U = 0$) marked as the black solid line, prominent intra-gap bound

states due to impurity pair-breaking occur close to the Fermi energy even for a small value of $U = 0.25$ (dash-dotted line). With increasing U , the two peaks move towards the Fermi energy and accidentally merge into a single sharp bound near zero energy as shown by the red solid line for $U = 0.4$. This nearly zero-energy bound state has already been observed in the $d_{x^2-y^2}$ -wave cuprate superconductors [30, 31]. In the unitary limit ($U = 50$), two intra-gap bound states reappear and locate symmetrically at the positive and negative energies, but the intensity of the two peaks are different due to the particle-hole asymmetry in the present β -band. When the inter-band impurity scattering is introduced, as seen in Fig. 4(b), two intra-gap bound states still exist with much higher spectrum intensities. This can be understood from the nodal structure of $d_{x^2-y^2}$ -wave as shown in the inset of Fig. 4(a). Since the nodal lines of the $d_{x^2-y^2}$ -wave cross undoubtedly the α - and β -FSs, both FSs contribute to the intra-gap bound states. However, because of the larger DOS of the corner corrugated heavy-electron β -band near the Fermi energy, its contribution to the intra-gap states is dominant. Hence the location of the intra-gap states are closer to the Fermi energy, and their intensities are much larger, in contrast to the case of loop-nodal s -wave pairing state considered above.

For comparison, the LDOS for the competitive fully gapped s -wave pairing is calculated and plotted in Fig. 5. For nodeless s^{++} -wave pairing without sign-changing in Fig. 5(a), it is clearly shown that the impurity-induced bound states emerge exactly at the gap edges. As expected, no intra-gap bound states can be induced by a nonmagnetic impurity even if the inter-band impurity scattering is included, which obeys the well-known Anderson’s theorem. However, since the sign-changing fully gapped s -wave SC state can be affected by impurities when considering the inter-band scattering, inclusion of the inter-band impurity scattering for the case of nodeless s^{\pm} -wave pairing as shown in Fig. 5(b) gives rise to two intra-gap bound states with symmetry respect to the

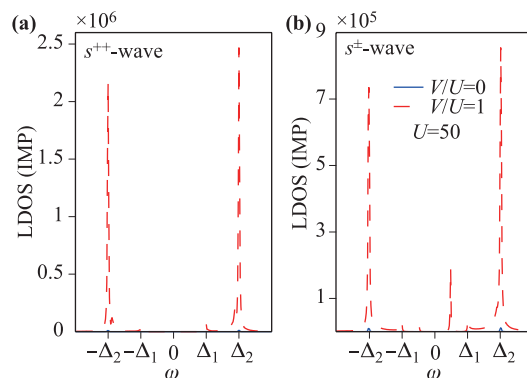


Fig. 5 The LDOS of quasiparticles at impurity site (IMP) for (a) the nodeless s^{++} -wave and (b) the nodeless s^{\pm} -wave pairing with only intra-band scattering ($V = 0$ and $U = 50$) and with both intra- and inter-band scattering ($V = U = 50$).

Fermi energy. This unique properties associated with the inter-band scattering might enable the STM measurement to verify the sign changing for the fully gapped s -wave pairing.

The impurity-induced low-energy quasiparticles will lead to characteristic signatures in scanning tunneling microscopy/spectroscopy, which has recently found quite successful in probing exotic properties in heavy fermion systems such as CeCoIn₅ [24, 25]. It is therefore quite appealing to also apply this technique to the heavy fermion superconductor CeCu₂Si₂. Given the above qualitative differences, we expect that the tunneling conductance in the STM experiment will provide a promising alternate to distinguish the possible gap structures of the SC gap function for CeCu₂Si₂ at ambient pressure.

4 Summary

In conclusion, we study the impurity scattering in the SC state of CeCu₂Si₂ at ambient pressure using an effective two hybridization-band model derived from the first-principles calculations. The resulting Fermi surfaces include a corrugated-cylindrical heavy electron sheet and a complex hole sheets, thus providing a basis for multiband superconductivity observed in experiment. Our calculations using the T -matrix approach for the effect of impurity scattering on the local electronic structures yield clear differences in the impurity bound states for the $d_{x^2-y^2}$ -wave, the nodal s -wave and the fully gapped s -wave (nodeless s^{++} and s^{\pm}) pairings. When only considering the intra-band impurity scattering, there exists no intra-gap bound states for the fully gapped s -wave, while impurity-induced intra-gap bound states for the $d_{x^2-y^2}$ -wave and the loop nodal s -wave are distinguishable and locate either near or far away from the Fermi energy, respectively. In addition, the inclusion of the inter-band impurity scattering could identify the sign changing or not for the fully gapped s -wave pairing. These qualitatively different features in the LDOS for different pairing states could be measured by future high-resolution STM experiment and thus provide a competitive way to shed light on the SC pairing in CeCu₂Si₂ at ambient pressure.

Acknowledgements This work was supported by the National Natural Science Foundation of China under Grant Nos. 11774025, 11774401, and 11522435. Y. Y. was also supported by the National Key R&D Program of China (Grant No. 2017YFA0303103) and the Strategic Priority Research Program (B) of the Chinese Academy of Sciences (Grant No. XDB07020200). S. F. was supported by the National Key R&D Program of China (Grant No. 2016YFA0300304).

References

1. F. Steglich, J. Aarts, C. D. Bredl, W. Lieke, D. Meschede, W. Franz, and H. Schafer, Superconductivity in the presence of strong pauli paramagnetism: CeCu₂Si₂, *Phys. Rev. Lett.* 43(25), 1892 (1979)
2. H. Q. Yuan, F. M. Grosche, M. Deppe, C. Geibel, G. Sparn, and F. Steglich, Observation of two distinct superconducting phases in CeCu₂Si₂, *Science* 302(5653), 2104 (2003)
3. F. Steglich, Twenty-five years of heavy-fermion superconductivity, *Physica B* 359–361, 326 (2005)
4. C. Bredl, H. Spille, U. Rauchschwalbe, W. Lieke, F. Steglich, G. Cordier, W. Assmus, M. Herrmann, and J. Aarts, Gapless superconductivity and variation of T_c in the heavy-fermion system CeCu₂Si₂, *J. Magn. Magn. Mater.* 31–34, 373 (1983)
5. J. Arndt, O. Stockert, K. Schmalzl, E. Faulhaber, H. S. Jeevan, C. Geibel, W. Schmidt, M. Loewenhaupt, and F. Steglich, Spin fluctuations in normal state CeCu₂Si₂ on approaching the quantum critical point, *Phys. Rev. Lett.* 106(24), 246401 (2011)
6. K. Ueda, Y. Kitaoka, H. Yamada, Y. Kohori, T. Kohara, and K. Asayama, ²⁹Si knight shift in the heavy-fermion superconductor CeCu₂Si₂, *J. Phys. Soc. Jpn.* 56(3), 867 (1987)
7. Y. Kitaoka, K. Ueda, K. Fujiwara, H. Arimoto, H. Iida, and K. Asayama, NMR investigation of superconductivity and Kondo-coherency in CeCu₂Si₂, *J. Phys. Soc. Jpn.* 55(3), 723 (1986)
8. K. Fujiwara, Y. Hata, K. Kobayashi, K. Miyoshi, J. Takeuchi, Y. Shimaoka, H. Kotegawa, T. C. Kobayashi, C. Geibel, and F. Steglich, High pressure NQR measurement in CeCu₂Si₂ up to sudden disappearance of superconductivity, *J. Phys. Soc. Jpn.* 77(12), 123711 (2008)
9. O. Stockert, J. Arndt, E. Faulhaber, C. Geibel, H. S. Jeevan, S. Kirchner, M. Loewenhaupt, K. Schmalzl, W. Schmidt, Q. Si, and F. Steglich, Magnetically driven superconductivity in CeCu₂Si₂, *Nat. Phys.* 7(2), 119 (2011)
10. H. A. Vieyra, N. Oeschler, S. Seiro, H. S. Jeevan, C. Geibel, D. Parker, and F. Steglich, Determination of gap symmetry from angle-dependent H_{c2} measurements on CeCu₂Si₂, *Phys. Rev. Lett.* 106(20), 207001 (2011)
11. I. Eremin, G. Zwicknagl, P. Thalmeier, and P. Fulde, Feedback spin resonance in superconducting CeCu₂Si₂ and CeCoIn₅, *Phys. Rev. Lett.* 101(18), 187001 (2008)
12. S. Kittaka, Y. Aoki, Y. Shimura, T. Sakakibara, S. Seiro, C. Geibel, F. Steglich, H. Ikeda, and K. Machida, Multi-band superconductivity with unexpected deficiency of nodal quasiparticles in CeCu₂Si₂, *Phys. Rev. Lett.* 112(6), 067002 (2014)
13. S. Kittaka, Y. Aoki, Y. Shimura, T. Sakakibara, S. Seiro, C. Geibel, F. Steglich, Y. Tsutsumi, H. Ikeda, and K. Machida, Thermodynamic study of gap structure and pair-breaking effect by magnetic field in the heavy-fermion superconductor CeCu₂Si₂, *Phys. Rev. B* 94(5), 054514 (2016)
14. M. Enayat, Z. Sun, A. Maldonado, H. Suderow, S. Seiro, C. Geibel, S. Wirth, F. Steglich, and P. Wahl, Superconducting gap and vortex lattice of the heavy-fermion compound CeCu₂Si₂, *Phys. Rev. B* 93(4), 045123 (2016)

15. G. M. Pang, M. Smidman, J. L. Zhang, L. Jiao, Z. F. Weng, E. M. Nica, Y. Chen, W. B. Jiang, Y. J. Zhang, H. S. Jeevan, P. Gegenwart, F. Steglich, Q. Si, and H. Q. Yuan, Fully gapped d -wave superconductivity in CeCu_2Si_2 , *Proc. Nat. Acad. Sci.* 115, 5343 (2018), arXiv: 1605.04786
16. T. Takenaka, Y. Mizukami, J. A. Wilcox, M. Konczykowski, S. Seiro, C. Geibel, Y. Tokiwa, Y. Kasahara, C. Putzke, Y. Matsuda, A. Carrington, and T. Shibauchi, Full-gap superconductivity robust against disorder in heavy-fermion CeCu_2Si_2 , *Phys. Rev. Lett.* 119(7), 077001 (2017)
17. Y. Li, M. Liu, Z. Fu, X. Chen, F. Yang, and Y. F. Yang, Gap symmetry of the heavy fermion superconductor CeCu_2Si_2 at ambient pressure, *Phys. Rev. Lett.* 120(21), 217001 (2018)
18. H. Ikeda, M. Suzuki, and R. Arita, Emergent loop-nodal s^\pm -wave superconductivity in CeCu_2Si_2 : Similarities to the iron-based superconductors, *Phys. Rev. Lett.* 114(14), 147003 (2015)
19. Ø. Fischer, M. Kugler, I. Maggio-Aprile, C. Berthod, and C. Renner, Scanning tunneling spectroscopy of high-temperature superconductors, *Rev. Mod. Phys.* 79(1), 353 (2007)
20. G. Knebel, D. Aoki, and J. Flouquet, Antiferromagnetism and superconductivity in cerium based heavy-fermion compounds, *C. R. Phys.* 12(5–6), 542 (2011)
21. G. Stewart, Non-Fermi-liquid behavior in d - and f -electron metals, *Rev. Mod. Phys.* 73(4), 797 (2001)
22. G. R. Stewart, Heavy-fermion systems, *Rev. Mod. Phys.* 56(4), 755 (1984)
23. P. Aynajian, E. H. da Silva Neto, A. Gyenis, R. E. Baumbach, J. D. Thompson, Z. Fisk, E. D. Bauer, and A. Yazdani, Visualizing heavy fermions emerging in a quantum critical Kondo lattice, *Nature* 486(7402), 201 (2012)
24. M. P. Allan, F. Masee, D. K. Morr, J. van Dyke, A. W. Rost, A. P. Mackenzie, C. Petrovic, and J. C. Davis, Imaging Cooper pairing of heavy fermions in CeCoIn_5 , *Nat. Phys.* 9(8), 468 (2013)
25. B. B. Zhou, S. Misra, E. H. da Silva Neto, P. Aynajian, R. E. Baumbach, J. D. Thompson, E. D. Bauer, and A. Yazdani, Visualizing nodal heavy fermion superconductivity in CeCoIn_5 , *Nat. Phys.* 9(8), 474 (2013)
26. B. Liu, Nonmagnetic impurity resonance states as a test of superconducting pairing symmetry in CeCoIn_5 , *Phys. Rev. B* 88(24), 245127 (2013)
27. G. Zhang, B. Liu, Y. Yang, and S. Feng, Spatial modulation of unitary impurity-induced resonances in superconducting CeCoIn_5 , *Front. Phys.* 11(3), 117402 (2016)
28. G. Zwicknagl and U. Pulst, CeCu_2Si_2 : Renormalized band structure, quasiparticles and co-operative phenomena, *Physica B* 186–188, 895 (1993)
29. A. V. Balatsky, I. Vekhter, and J. X. Zhu, Impurity-induced states in conventional and unconventional superconductors, *Rev. Mod. Phys.* 78(2), 373 (2006)
30. S. H. Pan, E. W. Hudson, K. M. Lang, H. Eisaki, S. Uchida, and J. C. Davis, Imaging the effects of individual zinc impurity atoms on superconductivity in $\text{Bi}_2\text{Sr}_2\text{CaCu}_2\text{O}_{8+d}$, *Nature* 403(6771), 746 (2000)
31. S. H. Pan, J. P. O’Neal, R. L. Badzey, C. Chamon, H. Ding, J. R. Engelbrecht, Z. Wang, H. Eisaki, S. Uchida, A. K. Gupta, K.W. Ng, E. W. Hudson, K. M. Lang, and J. C. Davis, Microscopic electronic inhomogeneity in the high- T_c superconductor $\text{Bi}_2\text{Sr}_2\text{CaCu}_2\text{O}_{8+x}$, *Nature* 413(6853), 282 (2001)